ISIJ International, Vol. 44 (2004), No. 8, pp. 1416–1425

Modeling of Austenite Grain Size Distribution in Nb Microalloyed Steels Processed by Thin Slab Casting and Direct Rolling (TSDR) Route

P. URANGA, A. I. FERNÁNDEZ, B. LÓPEZ and J. M. RODRIGUEZ-IBABE

CEIT and Tecnun (Univ. of Navarra), Pº M. Lardizábal, 15, 20018 Donostia-San Sebastián, Basque Country, Spain.
E-mail: jmribabe@ceit.es

(*Received on February 12, 2004; accepted in final form on May 7, 2004*)

A mathematical model has been developed to predict the austenite microstructure evolution of Nb microalloyed steels during "Thin slab casting" and "Hot direct rolling" (TSDR) processing. The model is based on empirical equations specifically derived for the microstructural and processing features typical in these new technologies. Its main novelty is that it works with austenite grain size distributions instead of the typical mean values as used in conventional models to represent the microstructure. This fact is particularly important in working with as-cast austenite due to the wide range of grain sizes present in this microstructure. In the model the different softening and hardening mechanisms that can operate during hot working in austenite are considered: static, dynamic and metadynamic recrystallization, grain growth after recrystallization and Nb(C, N) strain induced precipitation. The model uses the initial austenite grain size distribution as input and provides the size distribution of recrystallized and unrecrystallized grains at the entry of any rolling pass. A validation of the model has been carried out in the laboratory by multipass torsion tests. The model is capable of predicting any heterogeneities that may appear in the final microstructure after this kind of processing and that are not well predicted by using conventional models based on mean values. Additionally, it can calculate the deformation history, in terms of the strain accumulated in the austenite, and stress behavior, in terms of the mean flow stress (MFS) corresponding to each deformation pass.

KEY WORDS: thin slab direct rolling (TSDR); Nb microalloyed steels; microstructural modeling; grain size distribution; microstructural heterogeneity.

1. Introduction

"Thin slab casting", "Hot direct rolling" and "Hot charge rolling" are becoming more common in steel processing for the production of hot rolled flat or long products. These technologies have already proved to bring significant cost reductions. Although the thin slab casting and direct rolling (TSDR) have been successfully applied to the production of different steel grades, the use of this technology for higher steel grades, such as HSLA steels, is actually less. In this case, the adequate refinement of the austenite microstructure and particularly its microstructural homogeneity are very important factors in order to achieve high levels of strength and toughness.

The TSDR technology shows significant differences compared to conventional rolling processes. The metallurgical differences are mainly related to the coarse grain size ($\sim$1 mm) and the high supersaturation level of microalloying elements in as-cast austenite, in comparison to the as-reheated material ($\leq$250 μm).[1–4] Secondly, there are differences in the processing parameters. For example, the total number of rolling passes during TSDR is smaller, but usually the strains applied in the initial stands are higher.[3]

Ferrite grain refinement is considered the only procedure that brings a simultaneous improvement in the strength and toughness of ferritic microstructures. This microstructural refinement is usually obtained through an austenite conditioning prior to transformation by applying thermomechanical treatments. In the case of the TSDR the aforementioned process and microstructural singularities introduce some additional complexities in the thermomechanical treatment in comparison to conventional routes. If the parameters involved in the process, such as the initial hot rolling temperature, reduction grade in each stand, interstand times, chemical composition of the steel (mainly Nb and C contents) and total reduction during rolling, are not adequately combined important microstructural heterogeneities[1,5–7] can appear in the final product. When this occurs, it is possible to find wide zones within the ferrite–pearlite matrix that appear elongated in the rolling direction and made up of hard phases. Although they usually correspond to isolated features, their volume fraction can be high enough to significantly impair toughness.[8] The shape of these microstructural heterogeneities suggest that their origin might be related to the presence of some coarse austenite grains, probably inherited from the as-cast microstructure, that have remained unrecrystallized after the rolling process and become hard phases during subsequent cooling. As widely

reported[6,8–12] in the case of TSDR Nb microalloyed processed steels the final austenite microstructure might be ineffectively refined, creating a mixed ferrite structure with a wide range of grain sizes after transformation.

There are several factors that can affect the refinement of the as-cast microstructure in TSDR processes. On the one hand, the lower total strain applied on this route and on the other hand, the coarse as-cast austenite microstructure, can produce a retardation of static recrystallization kinetics during the first and second interstands of the direct rolling sequence compared to the conventional process.[2,4] This delay in recrystallization can give rise to partial recrystallized microstructures at the entrance of the following stand. Depending on the steel composition and rolling schedule, this incomplete recrystallization can remain during the entire rolling schedule, leading to heterogeneities in the final microstructure.[1,5–7] It should be pointed out that Nb microalloyed steel grades are more sensitive to this behavior, as a consequence of the solute drag effect of Nb and the precipitation of Nb(C, N) particles during rolling, both mechanisms able to significantly retard, and in some cases avoid, static recrystallization during the initial rolling stages.

In the last few years, much more attention has been paid to developing mathematical models to predict the final microstructure of a product based on the processing conditions. The aim of these models is to optimize the different variables in order to obtain as good a combination of strength-toughness properties in the as-rolled materials. Modeling has been also applied to TSDR processes, in some cases based on previously developed empirical equations for conventional rolling conditions[3,13–16] and in others incorporating specific equations obtained taking into account TSDR singularities.[1,3]

In a previous study[1] a mathematical model was developed for Nb microalloyed steels processed by the TSDR route. The model considers the influence of coarse austenite grain sizes and high supersaturation levels of microalloying elements on the recrystallization and precipitation kinetics.[4,17–19] A particularity of the model is that, taking into account the wide range of austenite grains sizes present in the initial as-cast microstructure,[1] it incorporates the initial austenite grain size distribution as input, instead of the mean value, and provides the size distribution of recrystallized and unrecrystallized grains at the entry of any rolling pass as outputs. Additionally, the following mechanisms interacting simultaneously are considered during hot rolling simulation: static recrystallization, grain growth during the interpass time and Nb(C, N) strain induced precipitation. With the introduction of these particularities, the model reasonably predicts, for a given chemical composition, processing conditions where an important fraction of coarse unrecrystallized austenite grains remains in the final microstructure prior to transformation.

However, as mentioned before, in the first rolling stands high strains are applied and this may cause dynamic recrystallization to start during deformation in TSDR processes. In fact, dynamic recrystallization has been proposed as one of the procedures that may be used to refine the as-cast microstructure during thin slab hot working.[3,20,21] Taking this into account, the previous model has been implemented by incorporating the effect of dynamic recrystallization and subsequent metadynamic softening during the interpass time.[22] The new model considers the initial austenite grain size distribution present in the TSDR technology and evaluates the interaction of the different softening mechanisms, static, dynamic and metadynamic recrystallization, with the strain induced precipitation of Nb carbonitrides, to predict the austenite grain size distribution after each rolling sequence. Laboratory simulations have been performed to test the austenite grain size distributions calculated by the model.

2. Model Development

2.1. Basis of Microstructural Model

The evolution of the austenite microstructure during rolling was modeled by equations based on mean grain size values and constant deformation parameters (strain per pass, strain-rate and temperature). For a specific deformation sequence, the model was applied for each deformation pass, calculating the microstructure at the entrance of the subsequent pass. The model is organized following a tree-structure, the depth being equal to the number of passes and each level is divided into two branches, the recrystallized and the unrecrystallized zones, respectively. These areas are treated independently for subsequent deformation, this method being reported in the literature as the law of mixtures.[19,23–26] This introduces the complexity of managing an increasing number of different structures throughout the deformation process. For the recrystallized volume fraction, X, it is assumed that the residual deformation is zero, while for the unrecrystallized fraction all the strain imparted in the previous pass is retained. Recrystallized and unrecrystallized zones are characterized by the values of the mean recrystallized, d_r, and unrecrystallized, d_u, grain sizes, respectively. As mentioned above, the possibility of dynamic recrystallization occurring during deformation was introduced now with respect to the previous model (detailed in Ref. 1)). This means that, apart from static recrystallization, metadynamic recrystallization must be also considered in modeling softening events after deformation.

Independently of the softening mechanism involved, partially recrystallized microstructures are characterized by the recrystallizing grain size, d_r. Theory predicts that if site saturation holds, there are no shape changes, the distribution of recrystallizing grains remains stable during recrystallization and no grain coarsening takes place, the evolution of the mean recrystallizing grain size d_r with time can be fairly described by the following relationship[27]:

$$d_r = d_{REX} \cdot X^{1/3} \quad \text{.....(1)}$$

where d_{REX} represents the final recrystallized grain size calculated for the corresponding post-dynamic softening mechanism, static (d_{SRX}) or metadynamic (d_{MDRX}) recrystallization, or a combination of both. Nevertheless, it has been reported that from a practical point of view Eq. (1) results appropriate to describe the evolution of d_r in a simple manner, even if theoretical conditions do not hold exactly.[19,27] The effective size of unrecrystallized grains, d_u, can be described with the help of the following expression proposed by Anelli[23]:

$$d_u = 1.06 D_0 \exp(-\varepsilon)(1-X)^{1/3} \quad \text{.....(2)}$$

where ε is the applied strain in each pass and X is the total recrystallized volume fraction: static (X_{SRX}), metadynamic (X_{MDRX}) or the sum of both. This equation takes into account both the flattening and the elongation of the original grains due to the applied deformation. Equations (1) and (2) were previously evaluated as a good procedure to predict the recrystallized and unrecrystallized grain size of coarse grained austenite microstructures, respectively.[19)]

In classical models, it is widely accepted that in the deformation range below the critical strain for the onset of dynamic recrystallization, $\varepsilon<\varepsilon_c$, the operating postdynamic softening mechanism is classical static recrystallization, while when $\varepsilon>\varepsilon_c$, dynamic recrystallization starts and postdynamic softening is governed by metadynamic recrystallization mechanisms.[3,15,28)] However, some recent works[29,30)] have shown that, for the case of Nb microalloyed steels, the characteristics of the metadynamic recrystallization kinetics (large effect of strain-rate and independence upon strain) are only achieved after some minimum strain, ε_T, is reached. In some specific conditions (coarse initial grain sizes) this strain value can be significantly larger than ε_c. For example, a relationship of $\varepsilon_T=2.2\varepsilon_c$ was found in a previous study[30)] carried out on a 805 μm sized Nb microalloyed steel. The origin of this singularity deals with the fact that metadynamic recrystallization only involves the growth of previously nucleated dynamic grains. If these grains are small in comparison to the original grains (as it occurs in TSDR processes), it is logical that a minimum fraction of dynamic recrystallized grains is required to obtain a complete softening by subsequent metadynamic recrystallization. This fraction has been observed to be close to 30–35% when the strain reaches the value of ε_T.[31,32)]

Consequently, there should be a transition between the strain range where static recrystallization operates as the main post-dynamic softening mechanism ($\varepsilon<\varepsilon_c$) and the point when metadynamic recrystallization intervenes ($\varepsilon>\varepsilon_T$). In the interval between both strains metadynamic recrystallization will start, but the completion of softening will require the activation of classical static recrystallization mechanisms in the remaining deformed zones.[30)]

These different softening mechanisms have been introduced into the model. The characteristic strains, ε_c and ε_T, both related to the peak strain, ε_p, are evaluated using the following relationships derived in previous papers[22,30)]:

$$\varepsilon_p = 3.7\times10^{-3}\,\frac{\{1+20([\mathrm{Nb}]+0.02[\mathrm{Ti}])\}}{1.78}\,D_0^{0.147}Z^{0.155} \quad \text{.....(3)}$$

$$\varepsilon_c = 0.77\varepsilon_p \quad \text{.....(4)}$$

$$\varepsilon_T = 2.2\varepsilon_c \quad \text{.....(5)}$$

where [Nb] and [Ti] represent the niobium and titanium concentrations in solution in wt%, D_0 the initial austenite grain size and Z is the Zener–Hollomon parameter calculated using an activation energy Q_{def}=325 kJ/mol.[22)] Depending on the relation between the applied strain and the characteristic strains ε_c and ε_T, the proper expressions for the recrystallized fraction, the time for 50% recrystallization, $t_{0.5}$, and the mean recrystallized grain size during interstand time are selected. The equations used in the model are indicated in **Table 1**. The parameter $t_{0.5}$ is used to determine the recrystallization kinetics by means of the usual Avrami type equation employed[4)]:

$$X = 1-\exp(-0.693(t/t_{0.5})^n) \quad \text{.....(6)}$$

where t is the time after deformation and n is a constant, which usually takes values between 1 and 2.[4,28)]

Three different regions of post-deformation softening behavior have been distinguished as a function of the applied strain:

Range I ($\varepsilon<\varepsilon_c$): For strains lower than the critical strain, softening is due to classical static recrystallization mechanisms. In this range the Eqs. (a) and (b) of Table 1 are considered. These relationships were determined in a previous paper using a wide range of initial grain sizes (20–1 100 μm).[4)] D_0 represents the initial austenite grain size, ε and $\dot{\varepsilon}$ are the applied strain and strain-rate, respectively, and T is the deformation temperature in Kelvin. For Nb steels the kinetics of static recrystallization (X_{SRX}) is well described by the Avrami equation with an exponent n equal to 1.[4)]

Table 1. Post-dynamic softening equations in the different deformation ranges for the kinetics of recrystallization process and the mean recrystallized grain size.

Range I: ($\varepsilon<\varepsilon_c$) **Classical static recrystallization**		**Ref.**	**Range III: ($\varepsilon>\varepsilon_T$)** **Metadynamic Recrystallization**		**Ref.**
$t_{0.5SRX} = 9.92\times10^{-11} D_0 \varepsilon^{-5.6 D_0^{0.15}} \dot{\varepsilon}^{-0.53} \exp\left(\frac{180000}{RT}\right) \cdot \exp\left[\left(\frac{275000}{T}-185\right)\cdot([Nb]+0.374[Ti])\right]$	(a)	4	$t_{0.5MDRX} = 1.77\cdot10^{-6}\dot{\varepsilon}^{-0.62} exp\left(\frac{153000}{RT}\right)$	(c)	30
$d_{SRX} = 1.4\left(\frac{D_0^{0.56}}{\varepsilon}\right)$	(b)	17	$d_{MDRX} = 1370\left(\dot{\varepsilon}\exp\left(\frac{375000}{RT}\right)\right)^{-0.13}$	(d)	32
Range II: ($\varepsilon_c<\varepsilon<\varepsilon_T$) **Static + Metadynamic recrystallization**					**Ref.**
$X = X_{SRX} + X_{MDRX}$ $\begin{cases} X_{MDRX} = X_f^{MDRX}\left[1-\exp\left(-0.693\left(\frac{t}{t_{0.5MDRX}}\right)\right)\right] \\ X_{SRX} = X_f^{SRX}\left[1-\exp\left(-0.693\left(\frac{t}{t_{0.5SRX}}\right)\right)\right] \end{cases}$	(e) (f)		$\begin{cases} X_f^{MDRX} = \frac{\varepsilon-\varepsilon_c}{\varepsilon_T-\varepsilon_c} \\ X_f^{SRX} = 1-X_f^{MDRX} \end{cases}$	(g) (h)	30 30
$d_r = d_{r_{SRX}}\cdot X_{SRX} + d_{r_{MDRX}}\cdot X_{MDRX}$, with $d_{r_{SRX,MDRX}} = d_{SRX,MDRX}\cdot X_{SRX,MDRX}^{1/3}$				(i)	20

Range III ($\varepsilon > \varepsilon_T$): For strains higher than the transition strain, ε_T, metadynamic recrystallization operates. The Eq. (c) in Table 1, previously derived for Nb steels with initial coarse grain size,[30] is used to calculate $t_{0.5MDRX}$. The evolution of the recrystallized fraction, X_{MDRX}, obeys to the Avrami type Eq. (6) with an exponent n equal to 1. The mean metadynamically recrystallized grain size has been evaluated using the Eq. (d) (Table 1) proposed by Roucoules *et al.*[32] for Nb microalloyed steels.

Range II ($\varepsilon_c < \varepsilon < \varepsilon_T$): In the intermediate deformation range, between the critical strain and the transition strain, both softening mechanisms, static and metadynamic recrystallization, are operating simultaneously, and the overall softening can be calculated by the sum of the individual components involved. The contribution of each process to the overall softening is calculated by Eqs. (e) and (f) in Table 1 for metadynamic and static recrystallization, respectively.[30] In these equations the terms X_f^{SRX} and X_f^{MDRX} represent the final recrystallized fraction that can be achieved by each mechanism. These values are expected to change with strain and it is assumed that, at strains close to ε_c, static recrystallization will be the main contributor, whilst, as the strain approaches ε_T, softening will be principally due to metadynamic recrystallization. To take into account the effect of strain on the values of X_f^{MDRX} and X_f^{SRX} the Eqs. (g) and (h) are applied. Equations (e)–(h) of Table 1 were shown to reasonably predict the evolution of the recrystallized fraction with time when both, static and metadynamic recrystallization mechanisms are operating.[30] More details about this model can be found in Ref. 30). The calculation of the average recrystallized grain size in this intermediate deformation range requires the inclusion of both the statically and metadynamically recrystallizing grains. The law of mixtures applied for the corresponding recrystallized fraction was considered (see Eq. (i)[20]).

If the time between passes (t_{ip}) is long enough for the completion of static and/or metadynamic recrystallization, grain growth can take place. The kinetics of grain growth after recrystallization are described by the following equation:

$$d^m = d_{REX}^m + A \cdot t_{gg} \exp\left(-\frac{Q_{gg}}{RT}\right) \quad \text{.....(7)}$$

where d_{REX} represents the fully recrystallized grain size that results in the case of only one softening mechanism acts (d_{SRX} and d_{MDRX} given by Eq. (b) or (d)) or the mixture value defined by Eq. (i) of Table 1 when both mechanisms are operating simultaneously, A is a constant that takes different values depending on the material, Q_{gg} the activation energy for grain growth and t_{gg} is the time remaining after complete recrystallization is reached, assuming a value of 95% recrystallized fraction for this state, *i.e.* $t_{gg} = t_{ip} - t_{0.95REX}$. Although theory would indicate that $m \cong 2$, in practice higher values are found, particularly for short times.[33] In this work, the following parameter values proposed by Hodgson and Gibbs for Nb bearing steels have been used[34]: $m = 4.5$, $A = 4.1 \cdot 10^{23}$ μm/s, $Q_{gg} = 435$ kJ/mol.

The model of microstructural evolution also includes the interaction between recrystallization and strain induced precipitation. The time for 5% strain induced precipitation of Nb(C, N) is defined by Eq. (8), based on the Dutta–Sellars model.[35] This model considers classical theory of diffusion-controlled nucleation and the thermodynamics of the system. Constants of this equation were obtained by fitting experimental results including microstructural conditions similar to those found in thin slab casting and direct charging processes (coarse grain size and high supersaturation levels).[17] For the calculation of the solubility product, the Eq. (9) proposed by Irvine *et al.*[36] was considered. If during the interpass time, precipitation (defined by $t_{0.05p}$) starts before recrystallization is complete, the precipitation is assumed to be the controlling mechanism and the recrystallization is stopped, preventing further recrystallization of that unrecrystallized fraction after subsequent passes.

$$t_{0.05p} = 5.3 \times 10^7 [\mathrm{Nb}]^{-1} \varepsilon^{-1} Z^{-0.5} \times \exp\frac{270\,000}{RT} \exp\frac{1.3 \times 10^{10}}{T^3 \ln(k_s)^2},$$

$$Z = \dot{\varepsilon} \exp\left(\frac{341\,000}{RT}\right) \quad \text{.....(8)}$$

$$k_s = \frac{[\mathrm{Nb}]\left[\mathrm{C} + \frac{12}{14}\mathrm{N}\right]_{sol}}{10^{(2.26 - 6\,770/T)}} \quad \text{.....(9)}$$

All the previous equations were obtained under isothermal conditions. However, in industrial conditions, during the interpass time the temperature decreases continuously. To extend the previous isothermal equations to continuous cooling conditions the additivity rule has been used.[37] This approach was applied for recrystallization, precipitation and growth kinetics.

2.2. Model Application to Grain Size Distributions

The aim of the model is, not only to predict the mean grain size values, but also the microstructural heterogeneities. Accordingly, the model described in the previous section has been expanded considering as input the initial austenite grain size distribution, instead of the mean value. This structure requires working with volume fractions; therefore, the first step is to convert the metallographically measured initial two-dimensional (2-D) austenite grain size distribution into a three-dimensional one (3-D). This is done with the help of the method developed by Matsuura and Itoh[38] for any grain size distribution type.

The resultant 3-D grain size distribution is divided into n intervals (usually between 10 and 15 for computer calculation). Each interval i is defined by its mean grain size (calculated assuming a spherical geometry) and the corresponding volume fraction. During hot rolling, the microstructural evolution of each interval, considered as a homogeneous material, is calculated independently by applying the Eqs. (1)–(9) and Eqs. (a)–(i) of Table 1. A schematic diagram of the model for each discretized interval is shown in **Fig. 1**. The following data are obtained for each i interval: the recrystallized fraction, $[X]_i$, and grain size, $[d_r]_i$, and the unrecrystallized grain size, $[d_u]_i$, and the retained strain, $[\varepsilon_r]_i$, in the unrecrystallized fraction.

At the end of the first interpass, the overall recrystallized and unrecrystallized microstructures will be defined by the

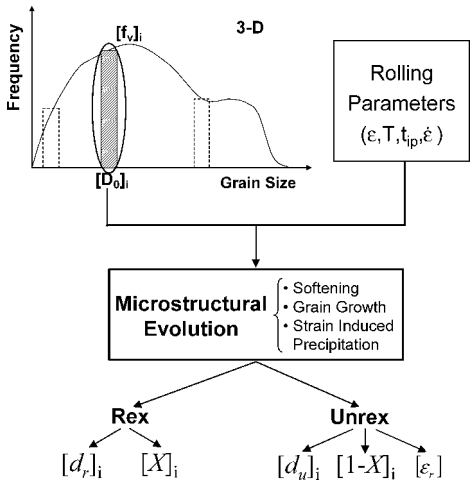

Fig. 1. Schematic diagram of the model for each discretized interval.

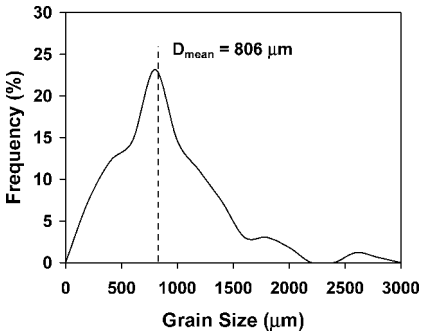

Fig. 2. Initial austenite grain size distribution determined in a Nb steel after reheating at 1 400°C during 15 min (torsion specimen).

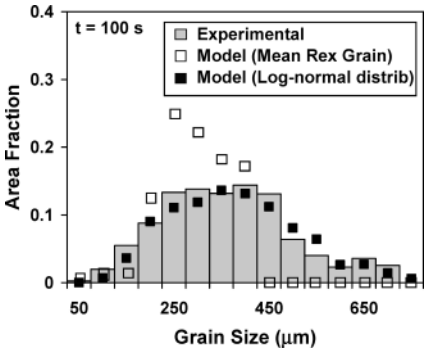

Fig. 3. Comparison between experimental metallographic measurements and model predictions for the austenite grain size distribution (T=1 100°C, ε=0.3, $\dot{\varepsilon}$=1 s^{-1}, deformed and then held 100 s), applying: mean recrystallized grain size (Eq. (b) of Table 1) for each initial interval (open symbols) and a log-normal distribution to each recrystallized grain size fraction (closed symbols).

sum of all the microstructures that result from the n intervals considered independently, each one weighted by its corresponding initial volume fraction.

The results obtained at the end of one interpass period are considered as the input for the next rolling pass. Each data is analyzed separately, proceeding as in the first pass and considering that the unrecrystallized material retains all the deformation applied in the previous pass, as indicated by the law of mixtures method.[23–26] This procedure is repeated all along the rolling sequence.

The model allows also the calculation of the deformation history. The average retained strain is determined after every interpass time as the sum of the strains retained at each unrecrystallized fraction calculated by the model:

$$\bar{\varepsilon}_r = \sum_{i=1}^{k} (1 - X_i) \cdot [\varepsilon_r]_i \quad \text{.....(10)}$$

where k is the total amount of final unrecrystallized fractions generated by the model.

3. Model Validation

The equations previously described were derived for mean austenite grain size values: therefore, before application of the model to industrial rolling conditions its validation for grain size distributions is necessary. Validation of the model was carried out with laboratory torsion tests using a Nb microalloyed steel with a composition (wt%): 0.1% C, 1.4% Mn, 0.035% Nb, 0.0053% N. Several situations were considered, taking into account the different post-deformation softening and hardening mechanisms that can operate during hot working.

3.1. Static Recrystallization

In the first validation step, hot working conditions where static recrystallization operates as the only post-dynamic softening mechanism were studied. Continuous torsion tests, carried out at isothermal conditions, were used to check the model predictions on statically recrystallized microstructures. The specimens were reheated at 1 400°C for 15 min, leading to the austenite grain size distribution shown in **Fig. 2**, which is comparable to those observed in industrial thin slabs.[1] After reheating, the specimens were cooled at 1°C/s to the deformation temperature of 1 100°C, and deformed applying a strain of ε=0.3 at a strain-rate of $\dot{\varepsilon}$=1 s^{-1}. The selected temperature was high enough to guarantee the absence of interaction with strain induced precipitation and the amount of strain was well below ε_c, the critical strain for the onset of dynamic recrystallization, so, only static recrystallization was involved. After deformation, the specimens were held at the deformation temperature for delay times varying from 10 to 100 s and then water-quenched in order to follow the evolution of the microstructure during static recrystallization. For each condition the recrystallized and unrecrystallized fractions and the corresponding grain size distributions were quantified metallographically.

Under these conditions, the predictions of the model agree to a large extent with the experimental measurements for the values of recrystallized volume fraction and size distributions of unrecrystallized grains. However, it fails to predict the recrystallized grain size distributions, as can be observed in **Fig. 3** (open symbols), where experimental measurements are compared with model predictions for a 100 s holding time, corresponding to a complete recrystallization state. The approach initially used, where each i interval has a mean recrystallized grain size value determined from Eqs. (1) and (b) to build the overall recrystallized grain size distribution, is inaccurate. As Fig. 3 denotes, the predicted distribution is limited to the 50–400 μm size range, while experimental values spread up to 700 μm. In order to overcome the limitation, for each i interval, a grain size distribution of recrystallized grains must be considered instead of a one mean value. To build these individual distributions, the following two aspects were taken into account:

– The grain size distributions of recrystallized microstructures can be properly described by log-normal distributions.[39]
– Experience shows that for the case of recrystallized mi-

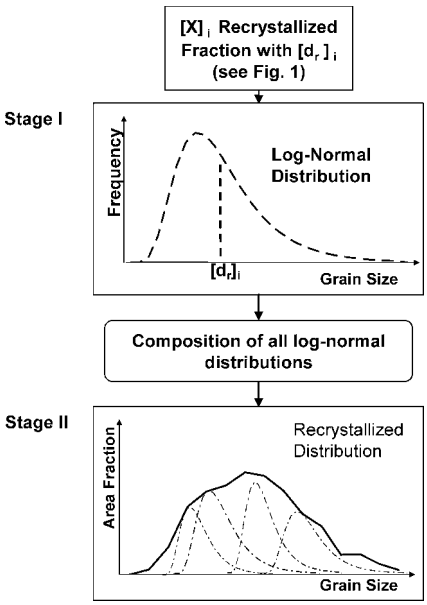

Fig. 4. Determination of the recrystallized grain size distribution after each pass through the composition of all log-normal distributions.

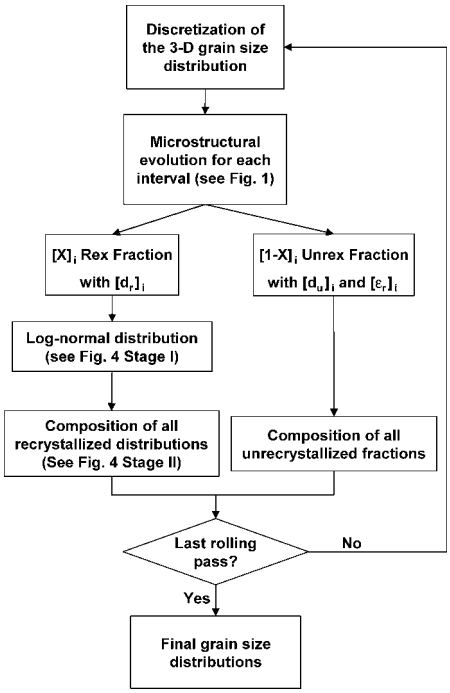

Fig. 5. Flow chart to determine microstructural evolution model in TSDR route.

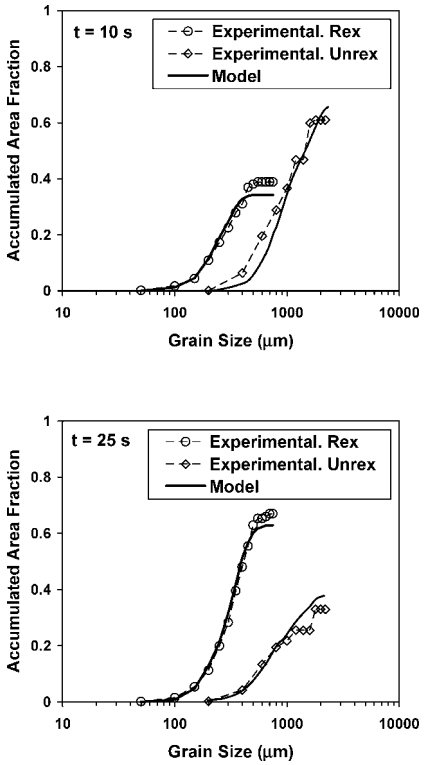

Fig. 6. Comparison between experimental metallographic measurements and model predictions for austenite grain size distributions for isothermal torsion tests (T=1 100°C, ε=0.3, $\dot{\varepsilon}$=1 s^{-1}). Two delay times after applied deformation have been considered: t=10 s and 25 s.

crostructures the maximum/mean grain size ratio stays between 3 and 4.[40)]

Consequently, a log-normal distribution of recrystallized grains was derived from each initial grain size interval. These log-normal distributions were built using a mean value equal to the one calculated from Eq. (b) and a maximum grain size 3 times larger than the mean one. Stage I of **Fig. 4** shows this procedure schematically. Once this modification is introduced in the model, the overall recrystallized microstructure is obtained again by the composition of all the resultant log-normal grain size distributions of the n intervals weighted by its corresponding initial volume fraction (Fig. 4 stage II). Flow chart to determine microstructural evolution model is shown in Fig. 5. For the case of unrecrystallized grains, the approach of consider for each i interval a unique mean unrecrystallized grain size applying Eq. (2) is enough. Consequently, the overall unrecrystallized grain size distribution will be defined by the composition of the results of the n intervals, each one weighted by its corresponding initial volume fraction.

As it was indicated previously, the results obtained at the end of one interpass period are considered as the input for the next rolling pass. Each data (recrystallized and unrecrystallized grain size distribution) is analyzed separately, proceeding as in the first pass (see Fig. 1) and considering that the unrecrystallized material retains all the deformation applied in the previous pass.[41)] The flow chart of the main model is shown in **Fig. 5**.

Figure 3 (closed symbols) shows that, after the modification of recrystallized microstructure for each i interval by a log-normal distribution and the subsequent composition, the predictions of the model for the recrystallized grain size distribution significantly improve. In order to check the validity of the model for partially recrystallized microstructures, two intermediate recrystallization stages corresponding to 10 and 25 s holding times were also studied. Model predictions and experimental results are compared in **Fig. 6** in terms of the accumulated area fractions, the latter evaluates the contribution of coarse grains better.[42)] A reasonable prediction is obtained for both recrystallized and unrecrystallized grain size distributions.

3.2. Metadynamic Recrystallization

In a second validation step, hot working conditions where dynamic recrystallization and subsequent metadynamic softening mechanisms might activate were studied. A continuous torsion test was performed applying a strain value of 0.93 at 1 080°C (soaking temperature 1 400°C, strain-rate 5 s^{-1}). This strain is larger than the ε_c critical strain for the onset of dynamic recrystallization, but far enough from ε_T (values of ε_c=0.81 and ε_T=1.85 were calculated for the selected testing conditions by using equations 3–5). After deformation the sample was continuously cooled at 5°C/s up to 1 000°C and then water quenched. Due to the impossibility of distinguishing between recrystallized and unrecrystallized grains, the resulting austenite grain size distribution was quantified without making any distinction between the different types of grains.

In **Fig. 7** the experimental grain size distribution has been compared to those predicted by the model taking into account two different modeling approaches. If the classical approach is considered (open symbols), *i.e.* assuming that

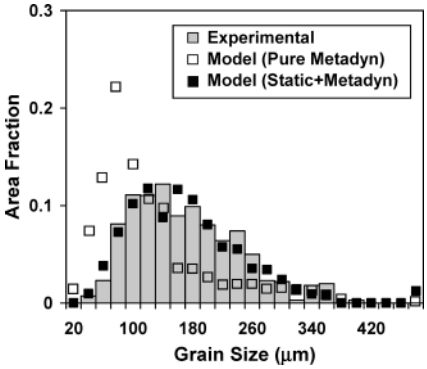

Fig. 7. Comparison between experimental measurements and model predictions of the austenite grain size distribution in the metadynamic recrystallization range. Open symbols: post-dynamic softening only governed by metadynamic recrystallization. Closed symbols: both classical static and metadynamic recrystallization mechanisms involved.

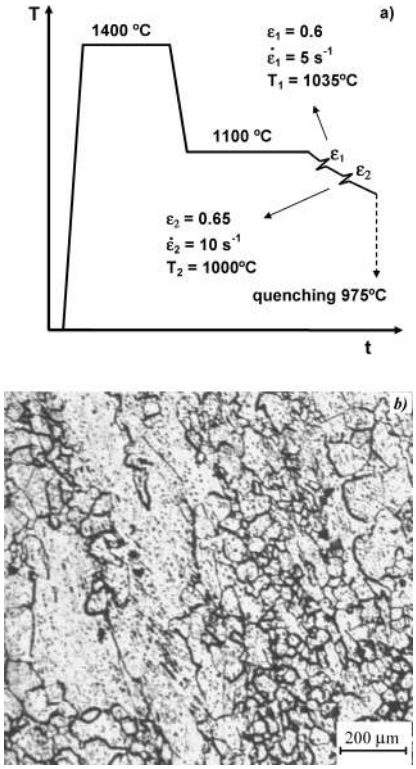

Fig. 8. (a) Scheme of the deformation schedule used for the third validation step (recrystallization-strain induced precipitation interaction); (b) microstructure after quenching at 975°C.

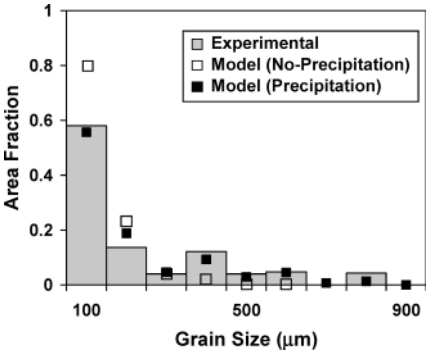

Fig. 9. Comparison between experimental measurements and model predictions for the austenite grain size distributions corresponding to the microstructure shown in Fig. 8. Closed and open symbols correspond respectively to considering or not interaction between precipitation and recrystallization.

once the strain reaches the critical ε_c value, the subsequent post-dynamic softening and grain size are governed exclusively by the equations corresponding to metadynamic recrystallization, the model predicts smaller grain sizes than those measured metallographically. This result can be explained by the fact that metadynamically recrystallized grain sizes are smaller than statically recrystallized ones (comparing Eq. (b) and Eq. (d)). In contrast, if the modifications mentioned in Sec. 2.1 for applied strains belonging to range II ($\varepsilon_c<\varepsilon<\varepsilon_T$) are considered, the prediction significantly improves, as shown in Fig. 7 (closed symbols). As can be observed in the figure, the agreement between the model and the experimental results is reasonable for all the grain size range. The model predicts that in this case the material recrystallizes almost completely, being the recrystallized fractions corresponding to each mechanism of $X_{SRX}=0.86$ and $X_{MDRX}=0.12$, respectively. The previous results denote that the classical approach (open symbols) would lead to significant errors in predicting the evolution of grain size after deformation for this coarse initial grain austenite.

3.3. Interaction between Post-dynamic Softening and Strain Induced Precipitation

Finally, deformation conditions where interaction between softening mechanisms and strain induced precipitation phenomena can take place were investigated. Double pass torsion tests were used for this validation step. The deformation schedule is shown schematically in **Fig. 8**(a). The torsion specimen was reheated at 1 400°C for 15 min and then cooled down to 1 100°C and maintained at that temperature for 20 min to simulate the equalization furnace step in TSDR. After this initial treatment, two deformation passes were applied during the continuous cooling of the specimen at a rate of ≈4°C/s. Deformation conditions are indicated in the figure. Some seconds after deformation the specimen was quenched for microstructural analysis. The resulting microstructure is shown in Fig. 8(b). From this microstructure the experimental grain size distribution was determined. As before, due to the difficulties of distinguishing between recrystallized and unrecrystallized grains (see Fig. 8(b)) this distribution was quantified without making any distinction between either type of grain.

Figure 9 shows the experimental grain size distribution compared to those predicted by the model assuming two different conditions: firstly, it is assumed that there is no interaction between recrystallization and precipitation (open symbols) and secondly, it is supposed that recrystallization stops once strain induced precipitation has occurred (closed symbols). From the figure it is clearly evident that the latter assumption leads to much better predictions.

If precipitation is not taken into account, the model predicts partial recrystallization after the first pass ($X_{rex}=$ 47%), but nearly complete recrystallization after the second pass accompanied by a significant refinement of the microstructure. This picture is far from the real microstructure where about 20% of the grains are coarser than 300 μm.

On the other hand, the proposed model (closed symbols in Fig. 9) considering precipitation–recrystallization interactions accurately predicts the presence of these coarse

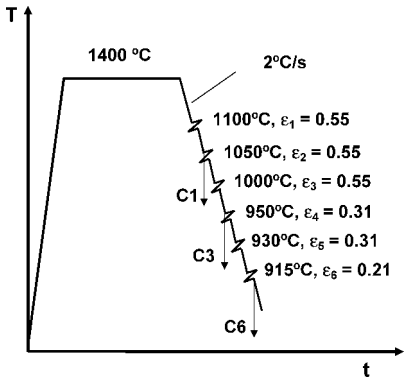

Fig. 10. Scheme of the deformation schedule applied for multipass rolling type simulation ($\dot{\varepsilon}=5\,s^{-1}$). C1, C3 and C6 represent the quenching stages.

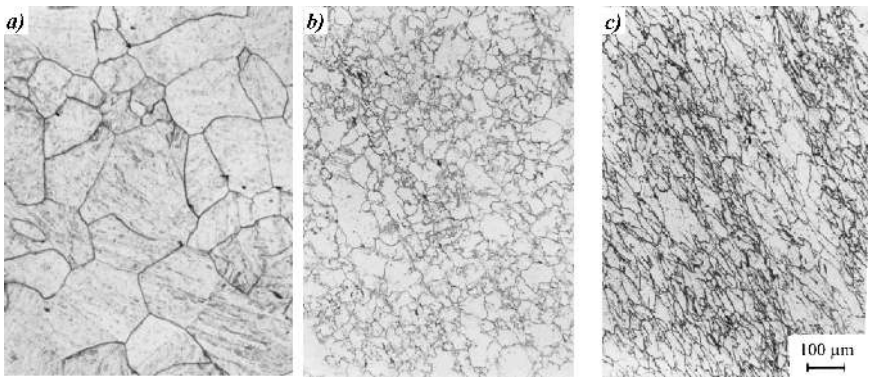

Fig. 11. Micrographs obtained on C1, C3 and C6 quenched samples in Fig. 10.

grains. In this case the model predicts that after the first pass, precipitation takes place at the end of the interpass interval ($t_{0.05p}=7$ s), at this moment the unrecrystallized fraction is close to $X_{unrex}=53\%$. It is assumed that this strain induced precipitation will mainly occur on unrecrystallized zones, further recrystallization of these zones is completely avoided after a subsequent pass. This explains the existence of an important fraction of coarse grains inherited from the initial coarse austenite that do not recrystallize during the process and remain in the final microstructure. After the second pass, the zones that have recrystallized during the previous interpass interval (47%) start recrystallizing again until precipitation takes place stopping the process. The model predicts an increasing of the unrecrystallized fraction up to about 70% due to the effect of precipitation after this second pass. Precipitation was confirmed by the analysis carried out by TEM using carbon replicas extracted from a specimen quenched after deformation. Small Nb(C, N) precipitates were identified, with a mean size of 10 nm, typical of strain induced precipitates.[43,44)]

4. Applications of the Model to Multipass Rolling Conditions

Finally, the applicability of the model to industrial rolling type sequences was investigated in order to completely validate it. Thermomechanical simulation was carried out in the laboratory with multipass torsion tests following the deformation schedule shown schematically in **Fig. 10**. The pass strains and interpass times used in this schedule are in the range of those employed in typical direct rolling processes, although it must be pointed out that in real industrial conditions the strain-rates can be significantly higher, with them being limited in the laboratory. Three samples were water-quenched at different stages during deformation for microstructural analysis; those denoted as C1 and C3 correspond to specimens quenched after the first and the third interpass times respectively, and C6 immediately after the sixth pass.

4.1. Austenite Grain Size Distribution

In **Fig. 11** the microstructures that come about after quenching in the three different stages mentioned are shown. **Figure 12** illustrates the grain size distributions calculated by the model compared to the experimental ones. It must be pointed out that as in previous analyses, experimental measurements have been performed without distinguishing between recrystallized and unrecrystallized areas. For the C1 sample the model predicts a completely recrystallized microstructure as is observed experimentally in Fig. 11(a). After the third interpass time (C3) the model predicts partial recrystallization (about a 66% recrystallized fraction) due to the interaction with precipitation. In the case of such high recrystallized fractions it is very difficult to distinguish in the microstructure what is recrystallized from what is not. However after the sixth pass, the austenite pancacking is clearly evident in Fig. 11(c). The model also predicts for this case a completely unrecrystallized microstructure. From Fig. 12 it can be also observed that the grain size distributions predicted by the model have a very good agreement with those experimentally measured.

The application of a mean grain size based model, as reported in Refs. 14) and 17), to the deformation sequence of Fig. 10 would lead to austenite grain size values of 109 and 32 μm for C1 and C3 quenching stages, respectively. These values are comparable to the mean values of 131 and 42 μm obtained for the model distributions in Fig. 12 at both stages; however, this figure clearly shows that in the microstructure there are grains significantly larger than these mean values. The advantage of the model proposed here is that it offers the possibility of modeling independently the microstructural evolution of all grain size ranges, and it is able to effectively predict the degree of microstructure homogeneity.

The microstructural heterogeneities present in the austenite prior to transformation can have a significant influence on the mechanical properties of processed materials, mainly on toughness. It is well established that the only microstructural parameter which can simultaneously improve strength and toughness is a reduction of the ferrite grain size, but to have a small ferrite grain is not enough to guarantee that a good combination of strength and toughness will be obtained. Several authors have analyzed the influence of the microstructure surrounding potential microcrack initiators (such as coarse non-metallic particles, cementites…) on the toughness, for some carbon steels.[45,46)] They have observed that cleavage fracture is directly related to the combination of microcracks and coarse microstructures. In the case of low carbon steels the ferrite grain size controls the propaga-

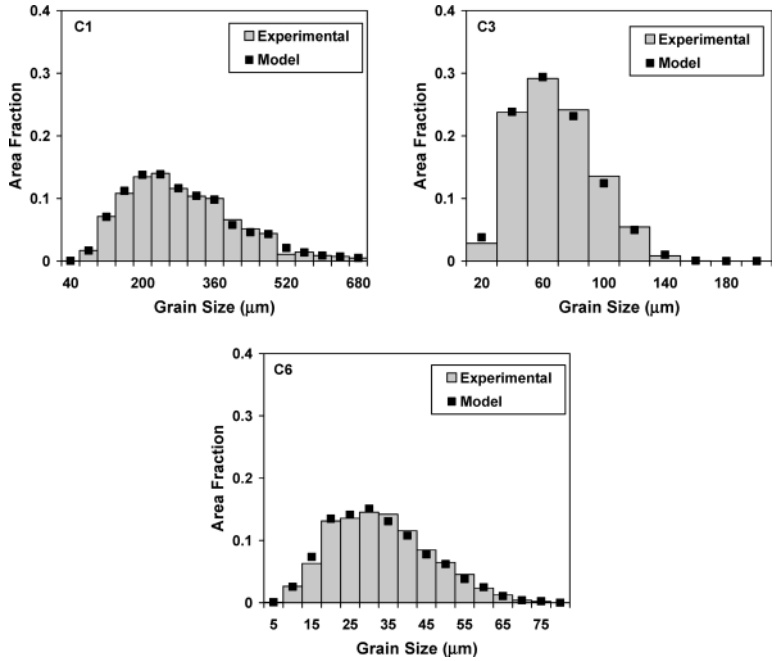

Fig. 12. Comparison of experimental measurements and model predictions for austenite grain size distributions at C1, C3 and C6 quenching stages in Fig. 10.

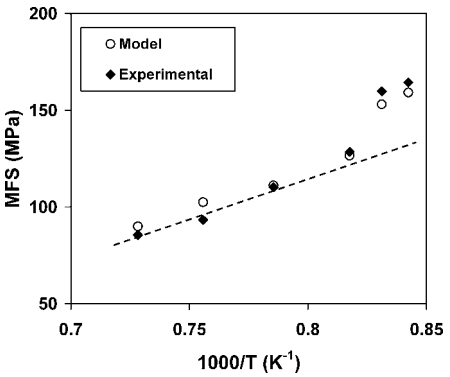

Fig. 13. Comparison between experimental mean flow stress values corresponding to the schedule shown in Fig. 10 and those predicted by the model, plotted as function of inverse absolute temperature.

tion of the microcracks through the matrix, the smaller the ferrite grain size the higher the minimum stress required for the crack to traverse the ferrite–ferrite grain boundary. As a consequence, a fine ferrite microstructure is very important in order to stop the cleavage process. However, it has been suggested that, independently of the mean ferrite grain size, toughness is controlled by the larger grain sizes in the distribution, according to the "weakest link" model.[47] Consequently, the possibility of predicting the overall grain size distribution in the austenite and subsequent ferrite microstructures can be very relevant from the point of view of modeling mechanical behavior, in order to get more accurate predictions of the mechanical properties.

4.2 Mean Flow Stress Validation

The validations of austenite grain size distributions have been done in the previous section, but the amount of accumulated strain value calculated by the model has not been checked. An indirect procedure to do that is to consider the mean flow stress values (MFS) relative to each deformation pass. This parameter is directly related to the rolling load and depends on the deformation history, being independent of the austenite grain size.

As it was mentioned previously, the model allows the calculation of the deformation history using Eq. (10), leading in the case of the schedule of Fig. 10 to a total average retained strain value of $\bar{\varepsilon}_r=0.78$. In the analyzed schedule the accumulation of strain can only be attributed to the retardation of recrystallization produced by strain induced precipitates, as solute drag mechanism is not strong enough for this.

The experimental determination of flow stress data from torsion testing is relatively straightforward. The MFS for each pass is determined from the area under the σ–ε curve normalized by the strain as follows:

$$\mathrm{MFS}=\frac{\int_{\varepsilon_a}^{\varepsilon_b}\sigma\cdot d\varepsilon}{\varepsilon_b-\varepsilon_a} \quad \text{.....(11)}$$

On the other hand, several methods have been proposed to calculate the mean flow stress as a function of composition and deformation parameters.[48,49] One of these is the Misaka equation,[49] which has often been employed to specify the MFS for C–Mn steels during hot strip rolling. Based on this equation a new modified Misaka equation that takes into account the effect of different alloying elements, such as Mn, Nb and Ti, was developed by Minami *et al*.[50] This relationship is displayed in Eq. (12).[50] It introduces strengthening factors for the different alloying elements present in solution in the austenite.

$$\mathrm{MFS}=9.8\exp\left(0.126-1.75[\mathrm{C}]+0.594[\mathrm{C}]^2+\frac{2\,851+2\,968[\mathrm{C}]-1\,120[\mathrm{C}]^2}{T+273.15}\right)\times(0.768+0.51[\mathrm{Nb}]+0.137[\mathrm{Mn}]+4.127[\mathrm{Ti}])\varepsilon^{0.21}\dot{\varepsilon}^{0.13} \quad \text{.....(12)}$$

MFS depends also on deformation parameters, *i.e.* the amount of strain and strain-rate, both variables included in Eq. (12). When deformation is retained in the austenite, this must be taken into account for the calculations with the modified Misaka equation. Here the accumulated strains predicted by the microstructural model are introduced, in this case for the deformation sequence shown in Fig. 10. The mean flow stresses obtained from the experimental stress-strain curves were plotted against the inverse absolute temperature in **Fig. 13**. In the same chart MFS values, calculated using the modified Misaka equation, Eq.

(12) with the accumulated strain determined from Eq. (10), are also included for comparison. The agreement between both sets of values is fairly good.

Therefore, it can be observed that the proposed model is able to accurately predict the effect of the accumulation of strain between passes on the mean flow stress, reflected by the slope change after the third pass. Strain starts accumulating after this pass, due to strain induced precipitation in the unrecrystallized regions. Before the sixth pass, the unrecrystallized fraction reaches 100% due to massive precipitation.

5. Conclusions

(1) A model to predict the microstructural evolution during hot rolling of coarse grain sized austenite has been developed considering that post-dynamic softening can involve static and metadynamic recrystallization mechanisms, as well as the possible interaction of these softening events with strain induced precipitation during interstand intervals.

(2) The main particularity of the model is that it works with austenite grain size distributions instead of mean grain size values. It takes as input the initial austenite grain size distribution and gives as outputs the size distributions of recrystallized and unrecrystallized grains present at the entry of any rolling pass. This means accurate predictions about possible heterogeneities present in the final austenite microstructure before transformation.

(3) The model has been implemented to obtain the mean flow stress values corresponding to each deformation pass, taking into account composition and deformation history. Such determined mean flow stress values are in very good agreement with experimental ones, denoting that the model is able to correctly predict the effect of the accumulation of strain between passes on stress behavior.

Acknowledgements

The authors wish to thank to the Dept. of Economy at the Gipuzkoa County Council for partial funding of the research. P. U. gratefully acknowledges a research grant from the Basque Government.

REFERENCES

1) P. Uranga, A. I. Fernández, B. López and J. M. Rodriguez-Ibabe: Proc. of 43rd MWSP Conf., Vol. 39, ISS, Warrendale, PA, (2001), 511.
2) P. Patel, C. Zhou and R. Priestner: Proc. 3rd Int. Conf. on Recrystallization and Related Phenomena, Rex '96, ed. by T. R. McNelley, Monterrey, MIAS, Monterrey, (1996), 421.
3) C. A. Muojekwu, D. Q. Jin, I. V. Samarasekera and J. K. Brimacombe: Proc. of 37th MWSP Conf., Vol. 33, ISS, Warrendale, PA, (1996), 617.
4) A. I. Fernández, P. Uranga, B. López and J. M. Rodriguez-Ibabe: *ISIJ Int.*, **40** (2000), 893.
5) M. Imagumbai and H. Takechi: Proc. of the Int. Conf. Thermec '2003, ed. by T. Chandra *et al.*, Materials Science Forum, 426–432, Trans Tech Publications Ltd., Switzerland, (2003), 1157.
6) Y. Kamada, T. Hashimoto and S. Watanabe: *ISIJ Int.*, **30** (1990), 214.
7) A. A. Khan, R. Priestner, C. Zhou and A. K. Ibraheem: Proc. of the Int. Conf. Thermec '97, ed. by T. Chandra *et al.*, TMS, Warrendale, PA, (1997), 2209.
8) A. I. Fernández, P. Uranga, B. López and J. M. Rodriguez-Ibabe: Proc. ECF13: The 13th European Conference on Fracture, Fracture Mechanics: Applications and Challenges, Elsevier, Surrey, UK, (2000), CD-ROM.
9) L. D. Frawley, R. Priestner and P. D. Hodgson: Proc. of the Int. Conf. Thermec '97, ed. by T. Chandra *et al.*, TMS, Warrendale, PA, (1997), 2169.
10) R. K. Gibbs, R. Peterson and B. A. Parker: Proc. of Int. Conf. Processing, Microstructure and Properties of Microalloyed Steels, ISS-AIME, Pittsburgh, (1992), 201.
11) R. Priestner and C. Zhou: *Ironmaking Steelmaking*, **22** (1995), 326.
12) K. Kunishige and N. Nagao: *ISIJ Int.*, **29** (1989), 940.
13) S. J. Cobo and C. M. Sellars: *Ironmaking Steelmaking*, **28** (2001), 230.
14) A. I. Fernández, B. López and J. M. Rodriguez-Ibabe: Proc. of the Int. Conf. on Thermomechanical Processing: Mechanics, Microstructure and Control, ed. by E. J. Palmiere *et al.*, The University of Sheffield, Sheffield, (2003), 302.
15) H. Yu, Y. Kang, K. Wang, J. Fu, Z. Wang and D. Liu: *Mater. Sci. Eng. A*, **363A** (2003), 86.
16) S. V. Subramanian, G. Zhu, H. S. Zurob, G. R. Purdy, G. C. Weatherly, J. Patel, C. Klinkenberg and R. Kaspar: Proc. of the Int. Conf. on Thermomechanical Processing: Mechanics, Microstructure and Control, ed. by E. J. Palmiere *et al.*, The University of Sheffield, Sheffield, (2003), 147.
17) R. Abad, A. I. Fernández, B. López and J. M. Rodriguez-Ibabe: *ISIJ Int.*, **41** (2001), 1375.
18) P. Uranga, A. I. Fernández, B. López and J. M. Rodriguez-Ibabe: Proc. of Thermomechanical Processing of Steels, The Institute of Materials, London, (2000), 204.
19) A. I. Fernández, B. López and J. M. Rodriguez-Ibabe: *Scr. Mater.*, **46** (2002), 823.
20) P. Uranga, A. I. Fernández, B. López and J. M. Rodriguez-Ibabe: Proc. of 44th MWSP Conf., Vol. 40, ISS, Warrendale, PA, (2002), 945.
21) N. Fujita, T. Narushima, Y. Iguchi and C. Ouchi: *ISIJ Int.*, **43** (2003), 1063.
22) A. I. Fernández, P. Uranga, B. López and J. M. Rodriguez-Ibabe: *Mater. Sci. Eng. A*, **361A** (2003), 367.
23) E. Anelli: *ISIJ Int.*, **32** (1992), 440.
24) J. H. Beynon and C. M. Sellars: *ISIJ Int.*, **32** (1992), 359.
25) P. D. Hodgson, A. Brownrigg and S. Algie: Proc. of Recrystallization '90, ed. by T. Chandra, TMS, Warrendale, PA, (1991), 541.
26) P. Choquet, A. Le Bon and Ch. Perdrix: Proc. of 7th Int. Conf. on Strength of Metals and Alloys, ed. by H. J. McQueen *et al.*, Pergamon Press, New York, (1985), 1025.
27) P. L. Orsetti and C. M. Sellars: *Acta Mater.*, **45** (1997), 137.
28) C. M. Sellars: Hot Working and Forming Processes, ed. by C. M. Sellars *et al.*, Metal Society, London, (1980), 3.
29) D. Q. Bai, S. Yue and J. J. Jonas: Proc. of J. J. Jonas Symp. on Thermomechanical Processing of Steel, Met. Soc., Ottawa, Canada, (2000), 669.
30) P. Uranga, A. I. Fernández, B. López and J. M. Rodriguez-Ibabe: *Mater. Sci. Eng. A*, **345A** (2003), 319.
31) A. I. Fernández: PhD. Thesis, Univ. of Navarra, San Sebastián, Spain, (2001). (in Spanish).
32) C. Roucoules, S. Yue and J. J. Jonas: *Metall. Mater. Trans. A*, **26A** (1995), 181.
33) C. M. Sellars: *Ironmaking Steelmaking*, **22** (1995), 459.
34) P. D. Hodgson and R. K. Gibbs: *ISIJ Int.*, **32** (1992), 1329.
35) B. Dutta and C. M. Sellars: *Mater. Sci. Technol.*, **3** (1987), 197.
36) K. J. Irvine, F. B. Pickering and T. Gladman: *J. Iron Steel Inst.*, **205** (1967), 161.
37) D. Q. Bai, S. Yue, W. P. Sun and J. J. Jonas: *Metall. Mater. Trans. A*, **24A** (1993), 2151.
38) K. Matsuura and Y. Itoh: *Mater. Trans. JIM*, **32** (1991), 1042.
39) M. Militzer, A. Giumelli., E. B. Hawbolt and T. R. Meadowcroft: *Metall. Mater. Trans. A*, **27A** (1996), 3399.
40) A. I. Fernández, B. López and J. M. Rodriguez-Ibabe: *Metall. Mater. Trans. A*, **33A** (2002), 3089.
41) S. Choi, Y. Lee, P. D. Hodgson and J. S. Woo: *J. Mater. Proc. Technol.*, **125–126** (2002), 63.
42) B. Roebuck: *Mater. Sci. Technol.*, **16** (2000), 1167.
43) L. J. Cuddy: Proc. of Int. Conf. Thermomechanical Processing of Microalloyed Austenite, ed. by A. J. DeArdo *et al.*, TMS AIME, Warrendale, PA, (1982), 129.
44) S. S. Hansen, J. B. Vander Sande and M. Cohen: *Metall. Mater. Trans. A*, **11A** (1980), 387.
45) M. A. Linaza, J. L. Romero, I. San Martín, J. M. Rodriguez-Ibabe and J. J. Urcola: Fundamentals and Applications of Microalloyed Forging Steels, ed. by C. J. Van Tyne *et al.*, TMS, Warrendale, PA, (1996), 311.
46) A. Echeverría and J. M. Rodriguez-Ibabe: *Mater. Sci. Eng. A*, **346A** (2003), 149.
47) T. Lin, A. G. Evans and R. O. Ritchie: *Metall. Mater. Trans. A*, **18A** (1987), 641.
48) Y. Misaka and T. Yoshimoto: *J. Jpn. Soc. Technol. Plast.*, **8** (1967–1968), 414.
49) S. Shida: *Hitachi Res. Lab. Report*, (1974), 1.
50) K. Minami, F. Siciliano, Jr., T. M. Maccagno and J. J. Jonas: *ISIJ Int.*, **36** (1996), 1500.